Journal of Laboratory Chemical Education 2020, 8(2): 23-27
DOI: 10.5923/j.jlce.20200802.01

# Preparation and Photothermal Property of $Fe_3O_4$@Au Composites: Senior Undergraduate Material Chemistry Comprehensive Experiment

**Yan Shan*, Xue-gang Yu, Xiao-zhen Yuan, Zhaobo Wang**

College of Materials Science and Engineering, Qingdao University of Science and Technology, Qingdao, China

**Abstract** In this paper, a comprehensive experiment for senior students majoring in material chemistry was introduced, which aims to improve the experimental and scientific research abilities of undergraduates. $Fe_3O_4$ microspheres were prepared by hydrothermal process with $FeCl_3 \cdot 6H_2O$ as raw material and ethylene glycol as solvent and reductant. After $Fe_3O_4$ particles were modified by imidazoline surfactant quaternary ammonium salt of 2-undecyl-1-dithioureido-ethyl-imidazoline (SUDEI), Au nanoparticles were attached on the surface of $Fe_3O_4$ microspheres, and the $Fe_3O_4$@Au composites could be obtained. The composites were characterized by scanning electron microscope (SEM), energy dispersive spectrometry (EDS) and transmission electron microscope (TEM). The photothermal properties of the composites were also investigated. It was found that the composites showed good magnetic property and photothermal conversion property, and the corresponding conversion efficiency can reach up to 21.2%.

**Keywords** $Fe_3O_4$@Au composites, Hydrothermal process, Photothermal

## 1. Introduction

Cancer is one of the diseases with the highest mortality. Researchers around the world have been working to develop more accurate and faster diagnostic and therapeutic methods to combat cancer [1-2]. Many therapeutic approaches, such as, aggressive surgery, radiation therapy, chemotherapy and immunotherapy have been taken to solve it, but the huge side effects such as, causing harm to healthy cells, destroying the immune system make them less effective [3-4]. Recently, potothermal therapy (PTT) has received a great deal of attentions for the advantage of noninvasive, controllable, and targeted strategy to eliminate tumor cells [5-9]. Photosensitizers are selectively accumulated to the tumor site, and then near-infrared light is applied to the tumor area. During the illumination process, photosensitizers absorb near-infrared light and efficiently convert it into heat energy, which makes the tumor generate local high temperature (over 42℃), so as to achieve the treatment purpose [2,3]. Because the photosensitizer distribution of normal tissues around the tumor is very small, it will not produce excessive temperature and will not damage normal cells, which ensures its safety and effectiveness in treatment.

Obtaining the biocompatible and effective photosensitizers is the most important problem in NIR laser-induced photothermal treatment. So to develop a high conversion efficient photosensitizer has been the focus in photothermal therapy study. By far, the research of photothermal absorbers mainly focuses on noble metal nanostructures, carbon-based nanomaterials, organic compounds and copper-sulfur semiconductors. Each of them has its own advantages and disadvantages. For example, carbon nanomaterials and organic compounds have advantage of low toxicity, however their photothermal conversion efficiency is low, and meanwhile organic compounds show severe photobleaching [10-13]. Semiconductor nanostructures, like $Cu_{2-x}S$ nanocrystals (NCs) [14-16], $Cu_{2-x}Se$ NCs [17], and $W_{18}O_{49}$ nanowires [18] show good photostability, high photothermal conversion efficiency, but their high toxicity limit their applications.

Among the materials, gold nanostructures [19-21], such as gold nanoshell, nanocages, nanorods, and nanostars are the most studied ones because of their good biocompatibility and high photothermal conversion efficiency. In this present experiment, $Fe_3O_4$@Au nanocomposites with the structure of gold nanoparticles modified on the surface of $Fe_3O_4$ microsphere have been designed and prepared successfully. The excellent magnetic property and ideal biocompatibility of $Fe_3O_4$ microspheres could make this composite material achieving targeting, thus improving the detection accuracy.

* Corresponding author:
shanyan@qust.edu.cn (Yan Shan)
Published online at http://journal.sapub.org/jlce

The photo-thermal conversion temperature could reach up to 42℃, indicating the composites exhibit a great application prospect in the thermal therapy.

## 2. Experimental Procedure

### 2.1. Materials

$FeCl_3·6H_2O$ (CAS No.10025-77-1) was purchased from Tianjin Chemical Reagent Corporation. Polyethylene glycol (CAS No.25322-68-3) and cetyl trimethyl ammonium bromide (CTAB, CAS No.57-09-0) were purchased from Tianjin Basifu Chemical Limited Company. Ethyl alcohol (CAS No.64-17-5) was purchased from Yantai Sanhe Chemical Reagent Corporation. NaAc (CAS No.6131-90-4) and ascorbic acid (CAS No.50-81-7) were purchased from Tianjin Bodi Chemical Limited Liability Company. $HAuCl_4$ (CAS No.27988-77-8), $AgNO_3$ (CAS No.7761-88-8) and $NaBH_4$ (CAS No.16940-66-2) were purchased from Shanghai Chemical Reagent Corporation. SUDEI was prepared by our laboratory. All the reagents in the experiment were the analytical grade and used without further treatment.

### 2.2. Synthesis of $Fe_3O_4$ Microspheres

The magnetic particles were prepared by solvothermal method according to the reference [22]. First, 5 mmol of $FeCl_3·6H_2O$ was dissolve into ethylene glycol solution under the condition of ultrasound to form a stable and transparent solution. Some of NaAc and polyethylene glycol were added subsequently, and the mixture was stirred vigorously for 30 min approximately. Then the mixture was transferred to a teflonlined autoclave and heated to 200℃ for 10 h. Finally, the reaction product was cooled to room temperature and washed with alcohol then dried at 60℃ for 4 h. The waste liquid in the reaction process is poured into the recycling bucket.

### 2.3. Modification of $Fe_3O_4$ Microspheres

The above synthesized $Fe_3O_4$ (20 mg) was dispersed in deionized water with addition of SUDEI (0.65 g). After being sonicated for 30 min, the $Fe_3O_4$ microspheres were collected by centrifugation, and then dried. The obtained sample was denoted as $Fe_3O_4$ @SUDEI.

### 2.4. Synthesis of $Fe_3O_4$ Microspheres @Au Seed

First, 50 mL of 0.01M $NaBH_4$ solution was prepared under the condition of 0℃. Then CTAB (0.3650 g) was dispersed in ultrapure water (8.4 mL), under the condition of magnetic stir 1.0 mL $HAuCl_4$ (1.0 mg/mL) and 0.6 mL $NaBH_4$ were added to this solution subsequently. The above synthesized $Fe_3O_4$@SUDEI was mixed with this solution under the stirring for 4 h. The final product was collected by centrifuge and washed with distilled water and dried at 60℃. The waste liquid was poured into the recycling bucket.

### 2.5. Synthesis of $Fe_3O_4$ @Au Nanocomposites

In a flask, first 3.5 g CTAB was dissolve in 100 mL water, and then 2 mL $AgNO_3$ (0.004 M) and 2 mL $HAuCl_4$ (10 mg/mL) as well as 0.7 mL ascorbic acid were added to this solution subsequently. Finally, the synthesized $Fe_3O_4$@Au seed nanoparticles were added and stirred for 4 h. The final product was collected by centrifuge and washed with distilled water for several times and dried at 50℃.

### 2.6. Characterization

X-ray diffractometer (XRD, Dmax-ra, Rigaku) was used to gain the structure of $Fe_3O_4$ microspheres; Field emission scanning electron microscope (SEM, JSM-6700F) and transmission electron microscope (TEM, JEM-2000EX,) were used to observe the morphology of $Fe_3O_4$ microspheres and $Fe_3O_4$@Au nanocomposites.

To measure the photothermal conversion performances of $Fe_3O_4$@Au nanocomposites, a test device was built according to reference [14,15] as shown in Fig. 1. Firstly, the composites were dispersed in water to form a suspension (2 mg/mL). An 808 nm laser beam is irradiated on a quartz tube containing 1 mL suspension, and the temperature was recorded by a paperless recorder every ten seconds.

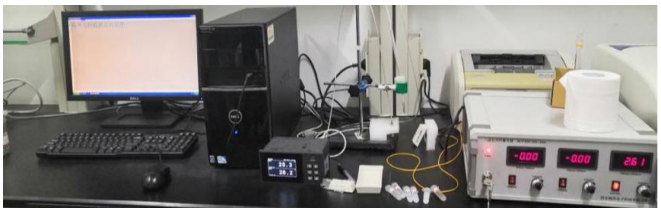

**Figure 1.** Photothermal conversion test device

The senior students were divided into several groups, such as material synthesis group, structure characterization group and photothermal properties test group. They were asked to take a presentation on project design, analysis and discussion of their results.

## 3. Results and Discussion

### 3.1. Structure and Morphology of $Fe_3O_4$ Microspheres

Figure. 2 is the XRD pattern, SEM and TEM image of the obtained $Fe_3O_4$ microspheres. From the XRD pattern, all the diffraction peaks can be indexed to $Fe_3O_4$ (JCPDS card No. 33-0311), indicating the products have good crystallinity and no other impurities exist. From the SEM image (b), it is found that the products were typical uniform aggregates of sphere with size mainly within 300~400 nm. The corresponding TEM image (c) showed that spherical particles with a hollow structure. According to the literature [23], the hollow structure was formed by the oriented aggregation and Ostwald ripening mechanisms.

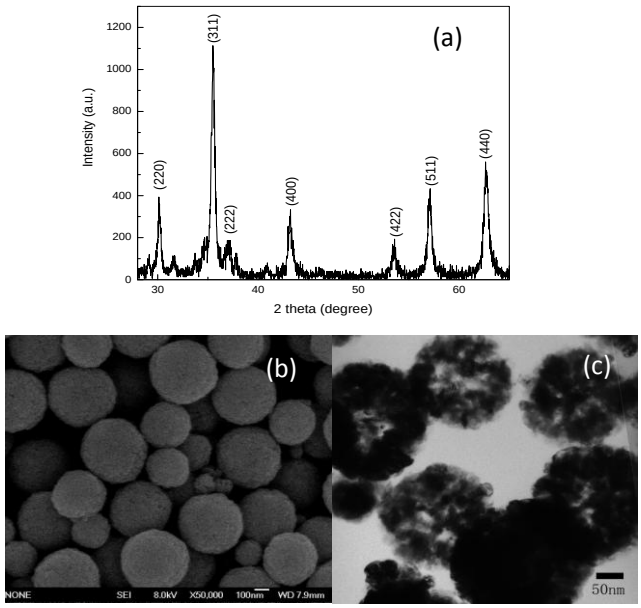


**Figure 2.** XRD pattern (a), SEM (b) and TEM image (c) of $Fe_3O_4$ microspheres

### 3.2. Morphology Characterization of $Fe_3O_4$@Au Nanocomposites

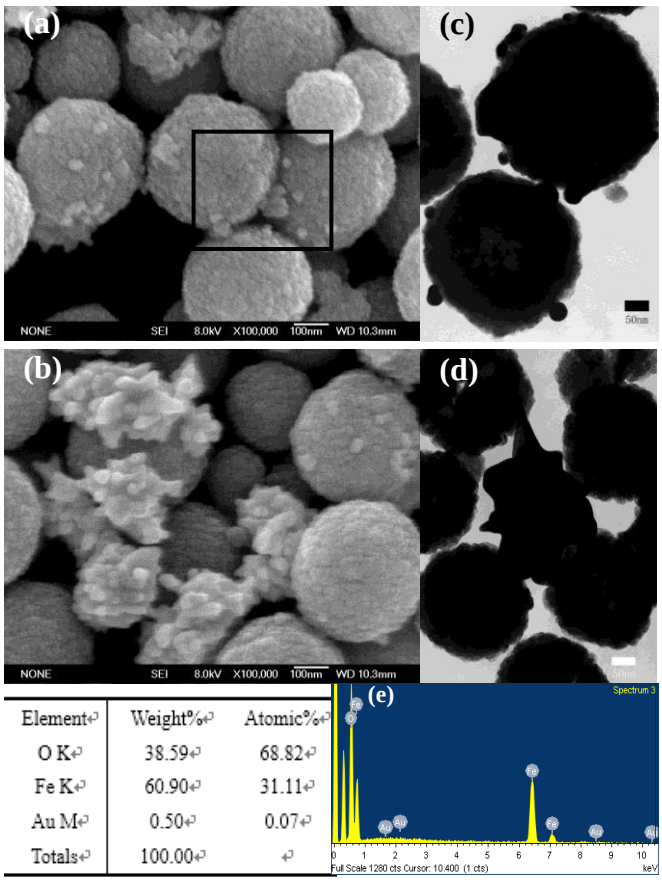


**Figure 3.** Micrographs and EDS analysis of $Fe_3O_4$@Au. (a) and (c) are the SEM and TEM images of $Fe_3O_4$@Au seed nanocomposites, (b) and (d) images are the SEM and TEM of $Fe_3O_4$@Au nanocomposites, (e) EDS spectrum of the selected area in (a)

The micrographs and EDS analysis of $Fe_3O_4$@Au are shown in Figure 3. Figure 3 (a) and (c) are the SEM and TEM images of $Fe_3O_4$@Au seed nanocomposites. From Figure 3 (a) and (c), it can be observed that there are several small particles with a size of 20 nm attached on the surface of $Fe_3O_4$. After the $Fe_3O_4$@Au seed product further growing in the solution of $HAuCl_4$, the $Fe_3O_4$@Au nanocomposites were obtained. The micrographs of $Fe_3O_4$@Au nanocomposites were shown as Figure 3 (b) and (d). From the SEM image of (b), the amount of Au nanoparticles was increased obviously, distributed on the surface of $Fe_3O_4$ microspheres, the corresponding TEM image was further confirmed that the morphology of Au nanoparticles was irregular with a size of 50 nm approximately. The EDS spectrum of selected area in (a) was shown as Figure 3(e), the product was composed of elements of Fe, O and Au, confirming the formation of $Fe_3O_4$@Au composites, and the content of element Au was 0.5%.

### 3.3. Synthesis Mechanism

The synthesis mechanism illustration of the prepared nanocomposites was shown in Figure 4. First, the $Fe_3O_4$ particles were modified by SUDEI, the structure of SUDEI was shown as follow:

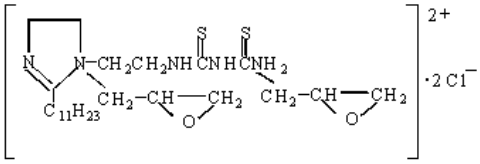

After modified by SUDEI, the surface of $Fe_3O_4$ particles had a mass of carbonyl sulfide groups and became positively charged. Au nanoparticles could easily be adsorbed on the surface of the modified $Fe_3O_4$ particles through the electrostatic attraction interaction and coordination action with carbonyl sulfide groups, thus $Fe_3O_4$@Au seed nanoparticles was formed. With the addition of $HAuCl_4$, Au seeds attached on the surface of $Fe_3O_4$ particles had a secondary growth preferentially, finally the $Fe_3O_4$@Au nanocomposites was synthesised successfully.

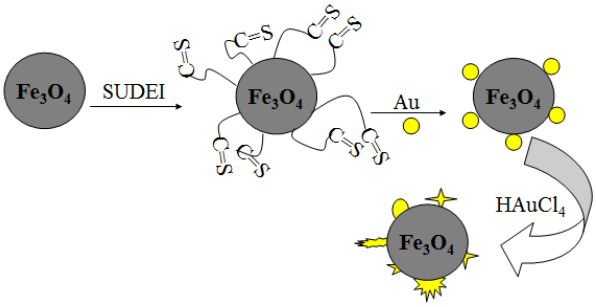


**Figure 4.** Synthesis mechanism of $Fe_3O_4$@Au nanocomposites

### 3.4. Photothermal Analysis of $Fe_3O_4$@Au Nanocomposites

$Fe_3O_4$ (20 mg) and $Fe_3O_4$@Au (20 mg) were respectively dispersed in the solution of CTAB to form stable suspension.

An 808 nm laser is irradiated on a quartz tube containing 1 mL suspension, and the temperature was recorded every ten seconds. The curve of Figure 5 from the bottom up were ultrapure water, CTAB solution, $Fe_3O_4$ suspension and the suspension of $Fe_3O_4$@Au composite, respectively. It was found that at the beginning all the solution's temperature increased rapidly with irradiation time, after more than 600 s, the heating rate became slowly and finally steady. Figure 5 showed that at the equilibrium state, the temperature of ultrapure water was 33℃, as well as CTAB solution. However, the temperature of $Fe_3O_4$ suspension could reach at 38℃ and the $Fe_3O_4$@Au composite could reach up to 40℃, which indicating the $Fe_3O_4$ and $Fe_3O_4$@Au have good photothermal property. $Fe_3O_4$ is black in color and can absorb infrared light strongly, so the photothermal property may be attributing to its lattice vibration. For $Fe_3O_4$@Au nanocomposites, in addition to the vibration of $Fe_3O_4$ lattice, more primarily, Au nanoparticles played an important role in this property, because there are a lot of free electrons in Au nanoparticles, and their ability of heat conduction is several times than the vibration of lattice. Therefore, although the content of Au was quite low, but this $Fe_3O_4$@Au nanocomposites had a better photothermal conversion efficiency. According to the relevant literature [16], the photo-thermal conversion efficiency (ŋ) of $Fe_3O_4$ and $Fe_3O_4$@Au nanocomposites were calculated:

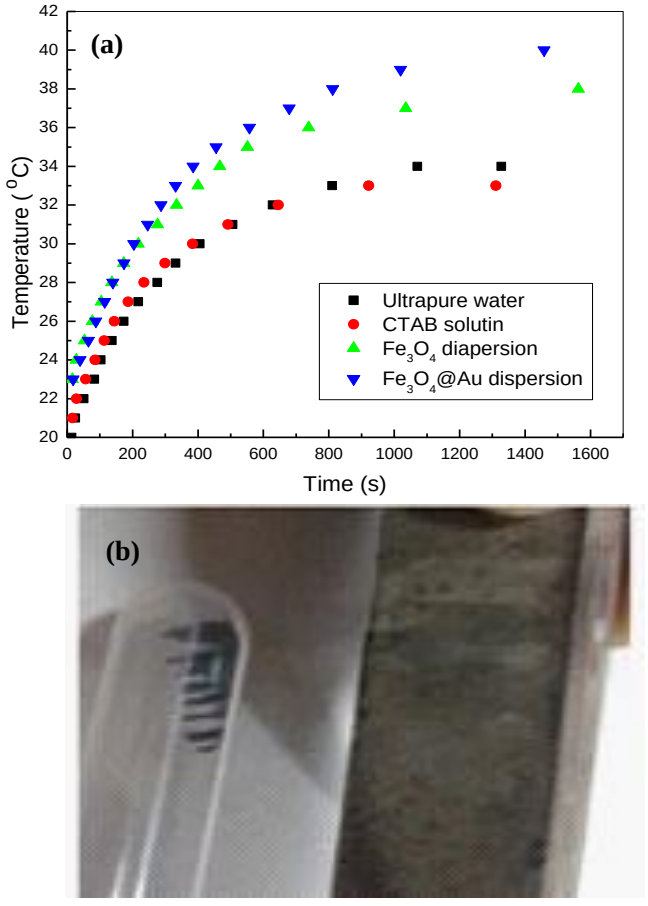


**Figure 5.** Photothermal conversion curve (a) of $Fe_3O_4$@Au and the digital photos of $Fe_3O_4$@Au responding to a magnet

$$\eta = \frac{\triangle T_{sample}}{T_{reference}} \quad (1)$$

In the formula (1), ΔT sample represents the temperature difference at thermal equilibrium state between sample and reference, $T_{reference}$ represents the temperature of water at thermal equilibrium state. It can be calculated that the photo-thermal conversion efficiency of $Fe_3O_4$ suspension is 15.2%, and the $Fe_3O_4$@Au composite suspension could reach up to 21.2%. And the composites showed a good magnetic property, so the $Fe_3O_4$@Au composite has a great application prospect in thermal therapy.

## 4. Conclusions

In summary, the $Fe_3O_4$@Au nanocomposites were synthesized successfully and photothermal property was also investigated. Sphere-like $Fe_3O_4$ microspheres were prepared by a hydrothermal process, after modified by SUDEI, Au nanoparticles were adsorbed on the surface of these particles. The composites (2 mg/mL) had a high photo-thermal conversion temperature and the corresponding conversion efficiency could reach up to 21.2%, exhibiting a potential application prospect in photothermal therapy.

## ACKNOWLEDGEMENTS

This work was supported by Teaching Reform Research Project of Qingdao University of Science and Technology (2018MS01); University-Industry Collaborative Education Program (No.201902085008).

## REFERENCES

[1] Madani S Y, Naderi N, Dissanayake O, et al. A new era of cancer treatment: carbon nanotubes as drug delivery tools [J]. International Journal of Nanomedicine, 2011, 6 (1): 2963-2979.

[2] Liu Y, Bhattarai P, Dai Z, Chen X. Photothermal therapy and photoacoustic imaging via nanotheranostics in fighting cancer [J]. Chemical Society Reviews, 2019, 48, 2053-2108.

[3] Jaque D, Maestro L M, Del Rosal B, et al. Nanoparticles for photothermal therapies [J]. Nanoscale, 2014, 6 (16): 9494-9530.

[4] Vogel A, Venugopalan V. Mechanisms of pulsed laser ablation of biological tissues [J]. Chem. Rev, 2003, 103(2): 577-644.

[5] Zhang S, Cheng Y, Ren L, et al. Reparation and photothermal properties of prussian blue nanoparticles with different morphologies [J]. Chemical Journal of Chinese Universities, 2018, 39 (2): 359-366.

[6] Broek B V an De, Devoogdt N, D'hollander, A, et al. Specific cell targeting with nanobody conjugated branched gold

nanoparticles for photothermal therapy [J]. ACS Nano, 2011, 5(6): 4319-4328.

[7] Ren Q, Li B, Peng Z, et al. SnS nanosheets for efficient photothermal therapy [J]. New J.Chem., 2016,40, 4464-4467.

[8] Tao W, Zhu X, Yu X, et al. Black Phosphorus Nanosheets as a robust delivery platform for cancer theranostics [J]. Adv. Mater. 2017, 29, 1603276.

[9] Xuan J, Wang Z, Chen Y, et al. Organic-base-driven intercalation and delamination for the production of functionalized titanium carbide nanosheets with superior photothermal therapeutic performance [J]. Angew. Chem. Int. Ed. 2016, 55, 14569 –14574.

[10] Yang J, Choi J, Bang D, et al. Convertible organic nanoparticles for near-infrared photothermal ablation of cancer cells [J]. Angew. Chem., Int. Ed. 2011, 50, 441-444.

[11] Yang K, Xu H, Cheng L, et al. In vitro and In vivo near-infrared photothermal therapy of cancer using polypyrrole organic nanoparticles [J]. Adv. Mater. 2012, 24, 5586-5592.

[12] Robinson J T, Welsher K, Tabakman S M, et al. High performance in vivo near-IR (> 1 μm) imaging and photothermal cancer therapy with carbon nanotubes [J]. Nano Res. 2010, 3, 779-793.

[13] Feng L, Yang X, Shi X, et al. Polyethylene glycol and polyethylenimine dual-functionalized nano-graphene oxide for photothermally enhanced gene delivery [J]. Small, 2013, 9 (11) 1989-1997.

[14] Tian Q, Jiang F, Zou R, et al. Hydrophilic $Cu_9S_5$ nanocrystals: A photothermal agent with a 25.7% heat conversion efficiency for photothermal ablation of cancer cells in vivo [J]. ACS Nano, 2011, 5(12): 9761-9771.

[15] Tian, Q, Tang, M, Sun, Y, et al. Hydrophilic flower-like CuS superstructures as an efficient 980 nm laser-driven photothermal agent for ablation of cancer cells [J]. Adv. Mater, 2011, 23, 3542- 3547.

[16] Wu D, Zhang C, Zhu H, et al. Sacrificial template synthesis and photothermal conversion enhancements of hierarchical and hollow $CuInS_2$ microspheres [J]. Physical Chemistry, 2013, 117, 9121-9128.

[17] Hessel C M, P. Pattani V, Rasch M, et al. Copper Selenide Nanocrystals for Photothermal Therapy [J]. Nano. Lett. 2011, 11, 2560-2566.

[18] Chen Z G, Wang Q, Wang H L, et al, Ultrathin PEGylated $W_{18}O_{49}$ nanowires as a new 980 nm-laser-driven photothermal agent for efficient ablation of cancer cells In vivo [J]. Adv. Mater. 2013, 25, 2095-2100.

[19] Cobley C M, Chen J Y, Cho E C, et al. Gold nanostructures: a class of multifunctional materials for biomedical applications [J]. Chem. Soc. Rev. 2011, 40, 44-56.

[20] Xia Y, Li W, Cobley C M, et al. Gold nanocages: from synthesis to theranostic applications [J]. Acc. Chem. Res. 2011, 44, 914-924.

[21] Bardhan R, Lai S, Joshi A, et al. Theranostic nanoshells: from probe design to imaging and treatment of cancer [J]. Acc. Chem. Res. 2011, 44, 936-946.

[22] Deng, H, Li X, Peng Q, et al. Monodisperse magnetic single-crystal ferrite microspheres [J]. Angew. Chem., Int. Ed. 2005, 117, 2482-2485.

[23] Jia B, Gao L. Morphological transformation of $Fe_3O_4$ spherical aggregates from solid to hollow and their self-assembly under an external magnetic field [J]. Phys. Chem, 2008, 112, 666-671.